Opto-Electronic Science

ISSN 2097-0382 CN 51-1800/O4

Periodic transparent nanowires in ITO film fabricated via femtosecond laser direct writing

Qilin Jiang, Long Chen, Jukun Liu, Yuchan Zhang, Shian Zhang, Donghai Feng, Tianqing Jia, Peng Zhou, Qian Wang, Zhenrong Sun and Hongxing Xu

Citation: Jiang QL, Chen L, Liu JK, Zhang YC, Zhang SA et al. Periodic transparent nanowires in ITO film fabricated via femtosecond laser direct writing. *Opto Electron Sci*, **2**, 220002(2023).

https://doi.org/10.29026/oes.2023.220002

Received: 11 February 2022; Accepted: 16 June 2022; Published online: 26 October 2022

Opto-Electronic Science

Article

January 2023, Vol. 2, No. 1

DOI: 10.29026/oes.2023.220002

Periodic transparent nanowires in ITO film fabricated via femtosecond laser direct writing

Qilin Jiang[1], Long Chen[1]*, Jukun Liu[1], Yuchan Zhang[1], Shian Zhang[1], Donghai Feng[1], Tianqing Jia[1,3]*, Peng Zhou[2], Qian Wang[2], Zhenrong Sun[1] and Hongxing Xu[1]

This paper reports the fabrication of regular large-area laser-induced periodic surface structures (LIPSSs) in indium tin oxide (ITO) films via femtosecond laser direct writing focused by a cylindrical lens. The regular LIPSSs exhibited good properties as nanowires, with a resistivity almost equal to that of the initial ITO film. By changing the laser fluence, the nanowire resistances could be tuned from 15 to 73 kΩ/mm with a consistency of ±10%. Furthermore, the average transmittance of the ITO films with regular LIPSSs in the range of 1200–2000 nm was improved from 21% to 60%. The regular LIPSS is promising for transparent electrodes of nano-optoelectronic devices—particularly in the near-infrared band.

Keywords: transparent nanowires; periodic surface nanostructures; femtosecond laser direct writing; ITO film; anisotropic electrical conductivity

Jiang QL, Chen L, Liu JK, Zhang YC, Zhang SA et al. Periodic transparent nanowires in ITO film fabricated via femtosecond laser direct writing. *Opto-Electron Sci* **2**, 220002 (2023).

Introduction

Indium-tin oxide (ITO) films with a wide bandgap of 3.5–4.3 eV provide high electrical conductivity (~10^{-6} Ω·m) and transmittance (>85%) in the visible and near-infrared (NIR) wavelengths. Because of their unique optoelectronic properties, ITO films have been widely used as transparent electrodes for solar cells and liquid-crystal displays, and as anode coatings for organic light-emitting diodes[1–3].

Modulating the properties of ITO films by using appropriate preparation methods and parameters is important[3–5]. The commonly used methods for ITO films include chemical vapor deposition, magnetic sputtering, evaporative coating and pulsed laser deposition. The deposition parameters, such as the element doping concentration, gas atmosphere, ambient pressure and sintering temperature, significantly affect the optoelectronic properties. Parra-Barranco et al. prepared ITO films with anisotropic in-plane conductivity and dichroic behavior via electron-beam evaporation at oblique angles[6].

For half a century, laser-induced periodic surface structures (LIPSSs) have been intensively studied with the development of laser technology[7]. LIPSSs are classified into two types according to their periodic characteristics: low-spatial frequency LIPSSs (LSFLs, $\lambda/2$–λ) and high-spatial frequency LIPSSs (HSFLs, $<\lambda/2$). The LIPSS is a universal phenomenon, and has been demonstrated on the surfaces of metals, semiconductors and transparent

[1]State Key Laboratory of Precision Spectroscopy, School of Physics and Electronic Science, East China Normal University, Shanghai 200062, China; [2]Huawei Technologies Co, Ltd., Bantian Longgang District, Shenzhen 518129, China; [3]Collaborative Innovation Center of Extreme Optics, Shanxi University, Taiyuan 030006, China.

*Correspondence: L Chen, E-mail: lchen@phy.ecnu.edu.cn; TQ Jia, E-mail: tqjia@phy.ecnu.edu.cn

Received: 11 February 2022; Accepted: 16 June 2022; Published online: 26 October 2022

materials irradiated by linearly polarized lasers[5,8–14]. These periodic nanostructures can be used to efficiently modify the properties of materials and have many applications in surface coloring[15–18], birefringence optical elements[19,20], and surface wettability[21–23].

Fabricating LIPSSs on ITO films is a unique method for modulating the optical and electrical characteristics. Reinhardt et al. enhanced the robustness of an ITO film in a severe environment (i.e., strong acid) by fabricating LIPSS with a nanosecond laser, which was attributed to the mixture phase state of the substrate and ITO film[24]. However, the excessive heat generated by the nanosecond laser caused crystallization in the deep layer, increasing the resistivity of the ITO film[25]. Liu et al. reported the processing of LIPSSs on ITO films with a picosecond laser to improve the transmittance of infrared light while ensuring a low resistance[26]. Femtosecond laser nanostructured ITO-coated glass was used as both a liquid-crystal alignment layer and an electrode with high transparency in optoelectronic devices. Moreover, the angular orientation of the LIPSSs responded differently from one another to bias voltage[27]. Interestingly, femtosecond laser energy can be transferred to ITO films in an extremely short time with less residual heat than that of nanosecond or picosecond laser, and femtosecond laser direct writing is an efficient method for fabricating regular LIPSSs on ITO films[19,28].

In this study, the anisotropic electrical conductivity and transmittance in the visible and infrared range of ITO films fabricated via femtosecond laser direct writing were investigated. A femtosecond laser with a central wavelength of 1030 nm, pulse width of 190 fs, and repetition rate of 1 kHz was focused on an ITO film by a cylindrical lens. Periodic ablation, regular LSFLs and partly damaged LSFLs were formed in sequence on the ITO films by increasing the laser fluence. The ratio of the anisotropic electrical conductivity was adjusted in the range of 1–10.8 by varying the laser fluence in the range of 0–0.488 J/cm^2. Interestingly, regular large-area LSFLs were efficiently fabricated on the ITO film by changing the laser fluence in the range of 0.510–0.637 J/cm^2. These LSFLs exhibited the properties of nanowires; the resistance varied from 15 to 73 kΩ/mm with a consistency of ±10%. The element concentrations and the resistivity of the LSFL nanowires and the ITO film with different thicknesses were studied in detail. The results indicated that the resistivity of the LSFL nanowires was well maintained. Furthermore, the average transmittance of the ITO film with LSFL nanowires in the infrared band was increased by 197% compared with that of the initial ITO film.

Experimental

Setup for femtosecond laser direct writing of LIPSS

In the experiment, a femtosecond laser was used to generate laser pulses with a center wavelength of 1030 nm, pulse duration of 190 fs, repetition rate of 1 kHz, and single-pulse energy of 1 mJ (PHAROS, Light Conversion). The laser system had an attenuator, which was used to adjust the laser power, as shown in Fig. 1(a). The focal length of the cylindrical lens used in the experiment was 50 mm, and the focal spot was 15 μm (1/e^2) wide and 4 mm long, as shown in Fig. 1(b). A half-wave plate was used to align the laser polarization parallel to the x-axis. The sample was placed on an electronically controlled three-axis translation stage. During laser fabricating LSFLs, the laser was scanning along the x-axis direction, and the ripples of LSFLs were along the z-axis direction. Figure 1(b) shows the schematics of laser polarization, focal spot, scanning direction, transverse and longitudinal directions.

Monitor system 1 was composed of white-light source 1, CCD 1, and the dichroic mirror, which was used to image the laser processing in real time. Monitor system 2 was composed of white-light source 2, CCD 2, and the 50× telephoto objective, which was used to precisely adjust the laser focus and sample surface, and to observe the surface microstructures after laser direct writing without removing the sample.

Sample preparation

The sample used in the experiment was a commercial ITO film with a thickness of 185 ± 10 nm coated on a substrate of quartz glass. The sheet resistance was measured to be 7.07 Ω/sq, and the resistivity was 1.31 × 10^{-6} Ω·m. ITO films with different thicknesses of 30–1200 nm were also studied. Before laser irradiation, the sample was ultrasonically cleaned with different solvents[19]. The sample was washed with a 10% acetone solution for 15 min to remove the surface oil stains and then with a 10% ethanol solution for 20 min to remove the residual acetone on the surface. Then, it was washed with a large amount of deionized water for 30 min to remove the surface ethanol.

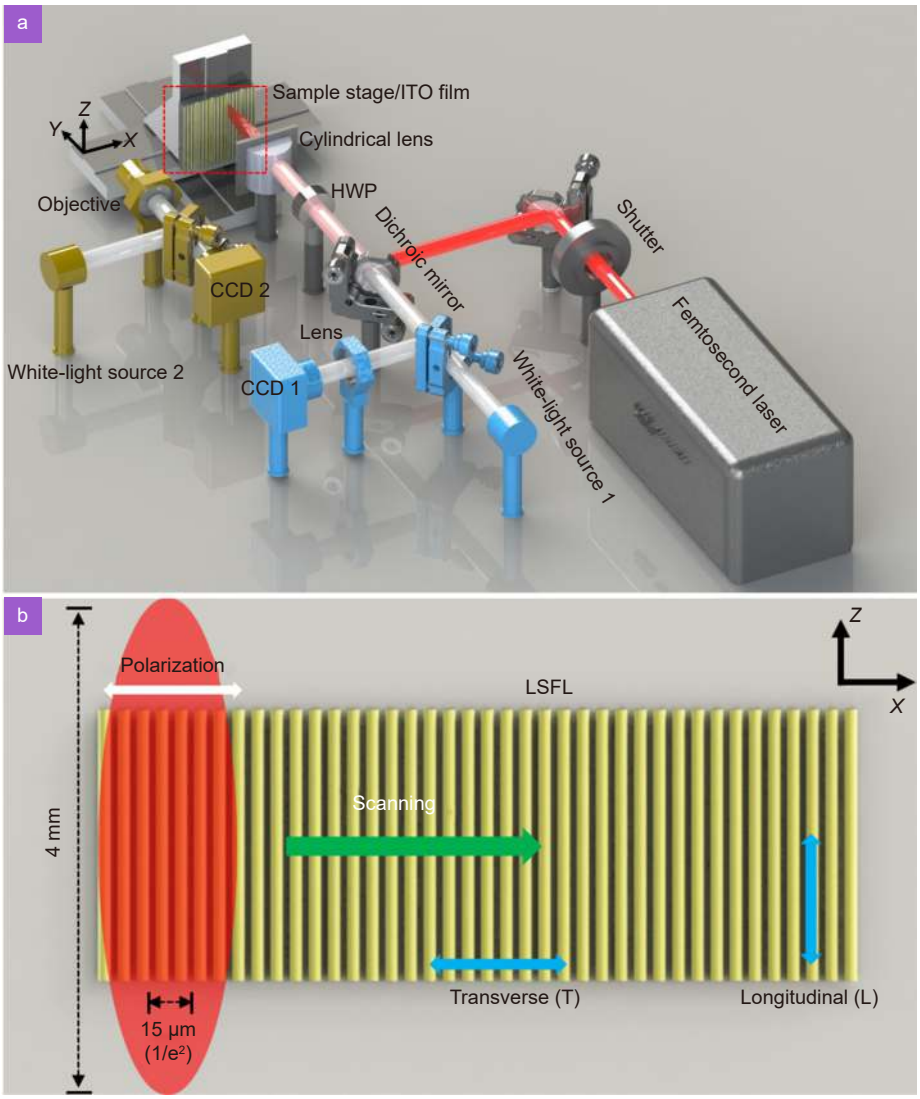

Fig. 1 | (**a**) Experimental system for direct writing of LIPSS in ITO films by a femtosecond laser. (**b**) Schematics of laser polarization, focal spot, scanning direction, transverse and longitudinal directions. HWP: half-wave plate, CCD: charge-coupled device.

Measurement of electrical properties of ITO film after laser direct writing

The electrical properties of the ITO film after laser direct writing were measured macroscopically via the four-probe method with a probe-tip diameter of 20 μm[29]. The resistance of a single nanowire was accurately measured via the dual-probe method. The probe-tip diameter was <500 nm. Details are presented in Supplementary information.

Measurement of surface morphology of ITO film after laser direct writing

The surface morphology was examined using a scanning electron microscope (SEM, Sigma 300, ZEISS) and an optical confocal microscope (Smartproof 5, ZEISS). Semi-quantitative measurement of the element contents was performed using energy-dispersive X-ray spectroscopy (EDS). The EDS instrument was an accessory of SEM and had an information depth of 600 nm.

Measurement of transmittance of ITO film after laser direct writing

The transmittance of the ITO film was measured using an UV–vis–NIR spectrophotometer (LAMBDA 950, PerkinElmer).

Results and discussion

Efficient fabrication of regular and large-area LSFLs

Laser processing parameters, including laser wavelength, fluence, and scanning speed, play crucial roles in the efficient and high-quality fabrication[30]. The transmittance of ITO film in the visible region is higher than 85%. When

processing thick ITO films, it is advisable to use a laser with a central wavelength in the visible region because of its deep penetration depth[31]. UV lasers could be chosen for the processing of LIPSSs with a shorter period. A commercial femtosecond laser with a central wavelength of 1030 nm was selected for the experiment. Compared with the 515 nm and 343 nm femtosecond lasers, the 1030 nm laser as the fundamental frequency laser has higher output power and is more stable. Moreover, the ITO film has a higher absorption rate, and the processed LIPSSs are regular, which are beneficial to industrial applications. Laser fluence and scanning speed are two key parameters for fabricating regular LIPSSs in ITO films[32]. In the following, the formation of LIPSSs is investigated in detail by varying the laser fluence and scanning speed.

Figure 2 shows SEM images of ITO films after laser direct writing with different fluences. The scanning speed was 3 mm/s. When the fluence was as low as 0.212 J/cm^2, as shown in Fig. 2(a), interval band-shaped ablation (periodic ablation) perpendicular to the laser polarization was observed. When the fluence increased to 0.446 J/cm^2, LSFLs perpendicular to the laser polarization appeared in the periodic ablation area. When the fluence increased to 0.531 J/cm^2, as shown in Fig. 2(c), a regular LSFL with a period of 929 nm was formed over the entire ablated region. When the fluence increased to 0.679 J/cm^2, the ridge of the LSFL fractured laterally, resulting in poor uniformity of the LSFL. In summary, three types of surface morphologies were formed on the ITO film surface by increasing the laser fluence: periodic ablation, regular LSFLs, and partly damaged LSFLs.

In addition to the significant effect of the laser fluence on the formation of the LSFL, the cumulative number of laser pulses has a substantial influence. Figure 3 presents the processing parameters (scanning speed and laser fluence) corresponding to the three aforementioned surface morphologies. At a higher speed, the fluence window was wider for the fabrication of a regular LSFL. For a scanning speed of 4 mm/s, the fluence window was as wide as 0.42 J/cm^2. However, the ridge height of the LSFL

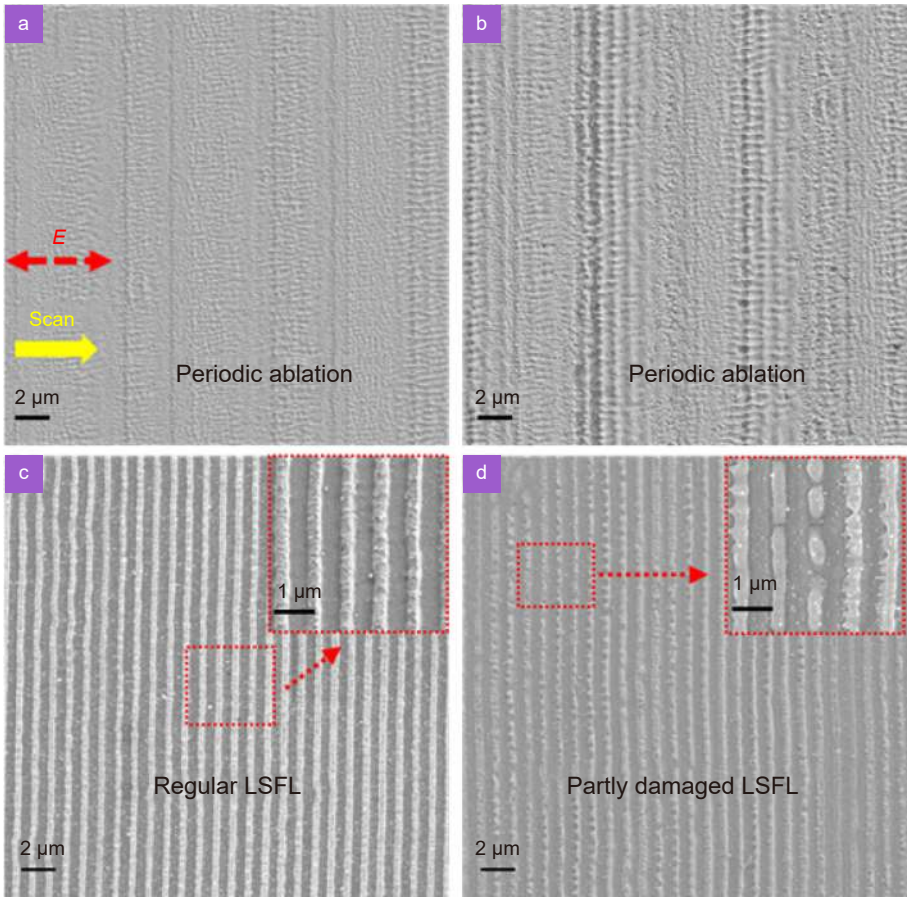

Fig. 2 | SEM images of ITO films irradiated by lasers with different fluences. (**a**) 0.212 J/cm^2, (**b**) 0.446 J/cm^2, (**c**) 0.531 J/cm^2, and (**d**) 0.679 J/cm^2. The inset shows an enlarged view of the area indicated by the red square. The scanning speed was 3 mm/s. The scanning direction and the direction of the electric field *E* are shown in (a).

was lower than those for scanning speeds of 2 and 3 mm/s. The fluence window for a regular LSFL was only 0.1 J/cm^2 when the scanning speed decreased to 1 mm/s, because of the excessive laser pulses. These results indicate that for efficiently fabricating regular and large-area LSFLs, a scanning speed of 3 mm/s is optimal.

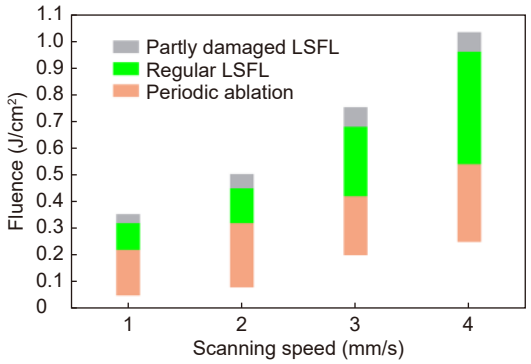

Fig. 3 | Laser fluences and scanning speeds for the three types of surface morphologies.

In the experiment, the cylindrical lens with a focal length of 50 mm was used, and the length of the focal spot was 4 mm. At the same scanning speed, the processing efficiency was improved by two orders of magnitude compared with that of a circular lens, which is beneficial for the preparation of large-area LSFLs. Figure 4(a) presents an SEM image of the large-area LSFL on the ITO film. The laser fluence was 0.552 J/cm^2, and the scanning speed was 3 mm/s. Figure 4(b) presents an enlarged SEM image corresponding to the red square in Fig. 4(a), and Fig. 4(c) shows the Fourier transform image of Fig. 4(b). The structures were regular, with a period of 929 ± 5 nm, and were perpendicular to the laser polarization direction. The depth of the LSFL was very consistent, with an average value of 207 ± 5 nm, which was slightly larger than the depth of the ITO film (185 ± 10 nm).

The thickness of pristine ITO film was about 185 nm, while the depth of LSFLs was about 200 nm. The deeper LSFLs were caused by two reasons. During laser ablation, the ITO material at the bottom of the valley was greatly ablated. Due to the eruption of ablated plume and thermal stress, part of the material was pushed towards the ridge, resulting in an increase in the depth of the LSFLs. Cheng et al and Zhou et al reported the formation of LSFLs by pump-probe imaging, clearly demonstrating the formation of LSFLs on Au thin films, and the

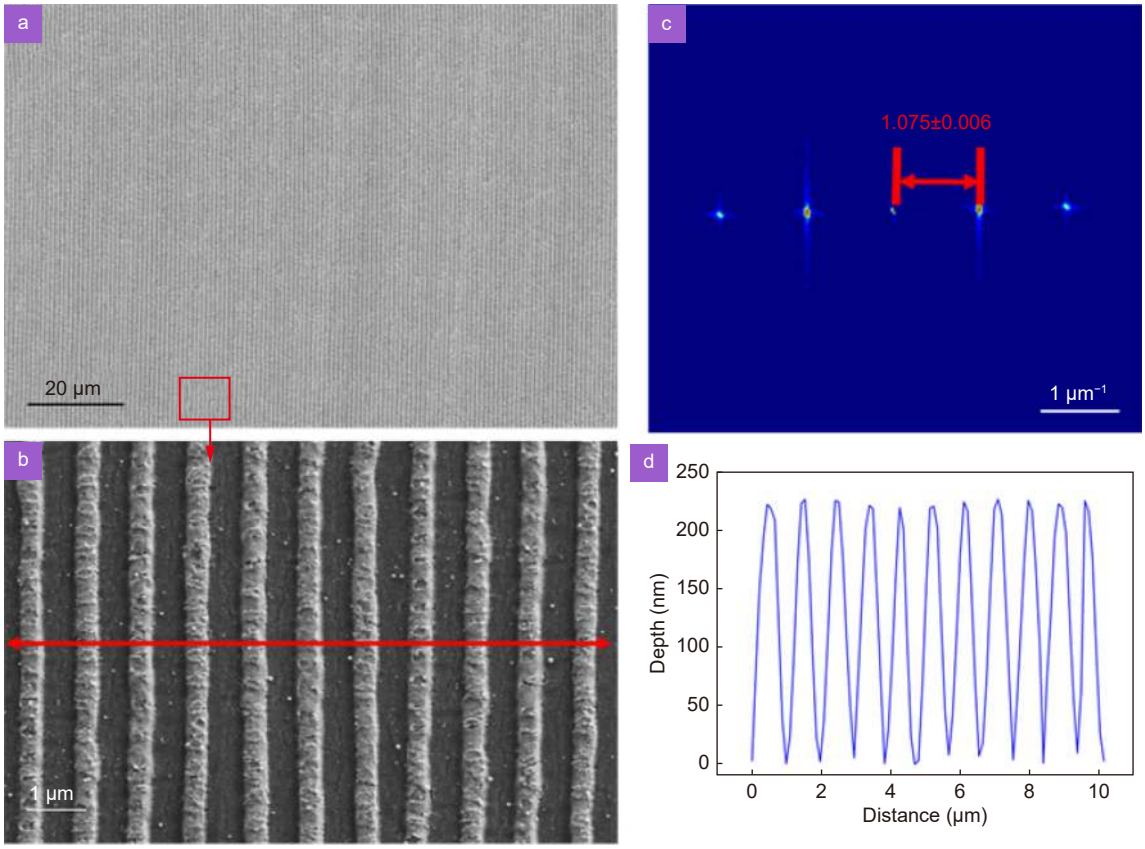

Fig. 4 | (**a**) SEM image of a large-area regular LSFL. (**b**) Enlarged image of the red square in (a). (**c**) Fourier transform image of (b). (**d**) Cross-sectional profile of the confocal optical micrograph of (b).

immersion caused by the molten surface layer[33,34]. Obvious bulges on both sides of the edge on ITO film were clearly observed after laser ablation[35,36], which further indicated that partial of the ablated material in the valley of LSFLs could be stacked on the ridges. Another reason is that there may be slight ablation of the substrate glass during the laser direct writing of ITO film, but it is not the main reason for the deepening of LSFLs, because the ablation threshold of ITO film was much smaller than that of glass[37,38].

Gratings in a large-area can be fabricated at one shot by two-beam interference of continuous wave (CW) laser. However, CW laser has strong material selectivity during processing, and it will bring large thermal effects during processing. The thermal effects will cause the gratings to be partially submerged as the material melts, resulting in shallower depths.

Regular gratings can be fabricated by femtosecond laser directing writing with two-beam interference[32,39]. Femtosecond laser has almost no material selectivity, and the thermal effect during processing is much smaller than that of CW laser. However, if a grating with a period of 929 nm is processed using two-beam interference of 1030 nm femtosecond laser, the cross angle between the two laser beams should be about 67°. For a 50 mm cylindrical lens, the focal spot width is only 15 μm, which means that if the sample is deviated by 5 μm in the front-to-back direction during processing, the focal spots of the two laser beams will be partly separated. Therefore, it is very difficult to fabricate grating in a large area by the two-beam interference of femtosecond laser. Moreover, the coherence of the two femtosecond lasers becomes poor due to the large cross angle, and the grating becomes shallower.

In the experiment, regular LSFLs with depths larger than 200 nm were efficiently processed by direct writing with single femtosecond laser. This processing method is simple, stable and efficient, and convenient for industrial promotion.

LSFL nanowires

The resistance of the ITO film is significantly affected by the surface morphology after laser direct writing. The resistance was measured along the longitudinal and transverse directions of the LSFL using the four-probe method[29]. The measured resistance was converted into the equivalent sheet resistance, as shown in Fig. 5.

The isotropous sheet resistance of the initial ITO film was measured to be 7.07 Ω/sq. When the laser fluence was < 0.212 J/cm², the sheet resistance changed little owing to the slight ablation, as shown in Fig. 5. When the laser fluence was > 0.23 J/cm², the sheet resistance increased rapidly. As shown in Fig. 2(b), the periodic ablation caused the transverse (T) and longitudinal (L) electrical conductivities to differ significantly. The spaced ablation reduced the electrical conductivity along the transverse direction, but hardly affected the electrical conductivity in the longitudinal direction. When the laser fluence increased to 0.510 J/cm², a regular LSFL was formed on the ITO film. As shown in Fig. 5, the corresponding sheet resistance was 7476 Ω/sq measured in the longitudinal direction, but the film was insulating in the transverse direction. The results of confocal optical microscopy indicated that the maximum depth of the LSFL was 220 ± 5 nm and that there was almost no ITO in the valley of the LSFL. In the range of 0.510–0.637 J/cm², the ITO film exhibited good unidirectional electrical conductivity. When the laser fluence was > 0.679 J/cm², the LSFL was broken, and the ITO film was insulating in both the longitudinal and transverse directions.

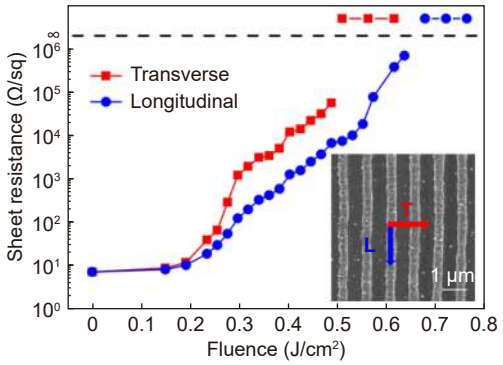

Fig. 5 | Sheet resistance of ITO film after laser direct writing with different fluences at a constant scanning speed of 3 mm/s.

Interestingly, the aforementioned results indicate that the ratio of the sheet resistances measured in the T and L directions can be tuned by varying the laser fluence. As shown in Fig. 6, when the laser fluence increased to 0.233 J/cm², the ratio slowly increased to 2.08. Subsequently, when the laser fluence increased to 0.297 J/cm², the ratio rapidly increased to 10.8. In the range of 0.297–0.488 J/cm², the ratio fluctuated between 8 and 11. The ratio increased abruptly to infinity in the range of 0.510–0.637 J/cm² because a regular LSFL was formed on the ITO film. These results indicate that by changing the laser fluence, the anisotropy of the surface electrical conductivity of ITO thin films can be adjusted, which can be useful in many fields[6,27].

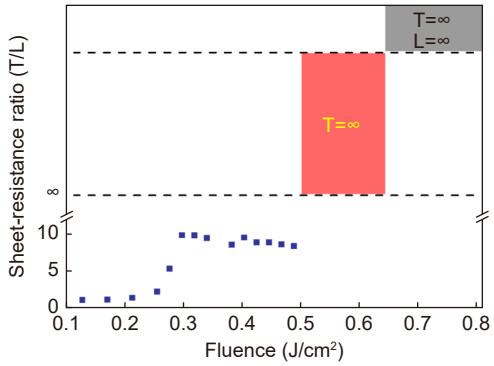

Fig. 6 | Ratio of the sheet resistance along the transverse (T) and longitudinal (L) directions with respect to the laser fluence at a constant scanning speed of 3 mm/s.

When the regular LSFL was fabricated on the ITO film, the ITO material was almost completely ablated in the valley. The LSFL exhibited unidirectional electrical conductivity and was considered to be composed of multiple nanowires. The resistivity of nanowires was measured via the dual-probe method (see Supplementary information). To check the consistency of the nanowire resistivity, 10 individual nanowires were measured separately. The resistivities were calculated using the widths, heights and lengths of the measured nanowires. As shown in Fig. 7, the resistivity of nanowires fabricated using a laser with a fluence of 0.510 J/cm^2 was 1.395 × 10^{-6} Ω·m on average, with a fluctuation within ±0.1×10^{-6} Ω·m. Figure 8 shows clearly that the nanowires were not very smooth, and even had tiny cracks on the surface. The width of the nanowires also varied slightly. Both the processing quality of LSFLs and the consistency of nanowire resistivity should be further improved[16,32].

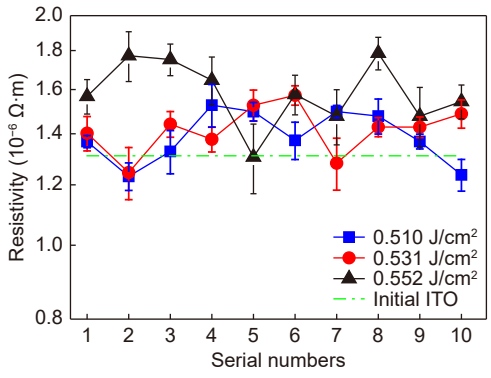

Fig. 7 | Resistivities of nanowires fabricated using lasers with different fluences.

When the laser fluence increased to 0.552 J/cm^2, the average resistivity increased to 1.590 ×10^{-6} Ω·m. The resistivity only increased by 6%–21% compared with the initial ITO film, indicating the high electrical conductivity of the nanowires fabricated via femtosecond laser direct writing.

Figure 8(a) shows SEM images of nanowires fabricated via laser direct writing with different fluences. The nanowire width decreased from 537 nm to 271 nm as the laser fluence increased from 0.510 J/cm^2 to 0.637 J/cm^2, as shown in Fig. 8(b). The nanowire height was measured via confocal optical microscopy, and it was reduced from 220 nm to 142 nm. The unit resistance of the nanowires fabricated using a laser with a fluence of 0.510 J/cm^2 was 15 kΩ/mm, as shown in Fig. 8(c). It increased to 73 kΩ/mm when laser fluence reached 0.637 J/cm^2 because the width and height both decreased. By adjusting the laser fluence, the unit resistance of a single nanowire could be changed over a wide range.

When the laser fluence increased from 0.510 J/cm^2 to 0.637 J/cm^2, the unit resistance of a single nanowire increased by a factor of 5. However, the resistivity increased from 1.395 × 10^{-6} Ω·m to 2.210 × 10^{-6} Ω·m (by only 62%). Therefore, the electrical conductivity of the nanowires fabricated using the femtosecond laser was well maintained.

Optical transmittance of ITO films after femtosecond laser direct writing

The bandgap of ITO could reach 3.5–4.3 eV, and the transmittance in the visible light band is >85%, as shown in Fig. 9[40]. The photon energy of ultraviolet light (λ < 355 nm) reaches or even exceeds the bandgap of ITO, resulting in higher absorption and lower transmittance. The reflection caused by the plasma vibration exhibited by electron-based carriers reduces the transmittance in the NIR region[4]. In addition to the electrical properties, the adjustment of the optical transmittance of the ITO film irradiated by a femtosecond laser is important[41]. Figure 9 presents the transmission spectra of the ITO film in the range of 250–2000 nm after laser direct writing with different fluences at a constant scanning speed of 3 mm/s.

The average transmittance of the 185-nm-thick ITO film in the range of 1200–2000 nm was 21.31%. The transmittance in the NIR band was significantly increased after the laser direct writing. When the laser fluence increased from 0.255 J/cm^2 to 0.318 J/cm^2, periodic ablation appeared on the ITO film, and the average transmittance in the infrared band increased from 26.57% to 33.05%. In the range of 0.318–0.425 J/cm^2, the periodic ablation became stronger, and the average transmittance in the infrared band increased to 44.17%.

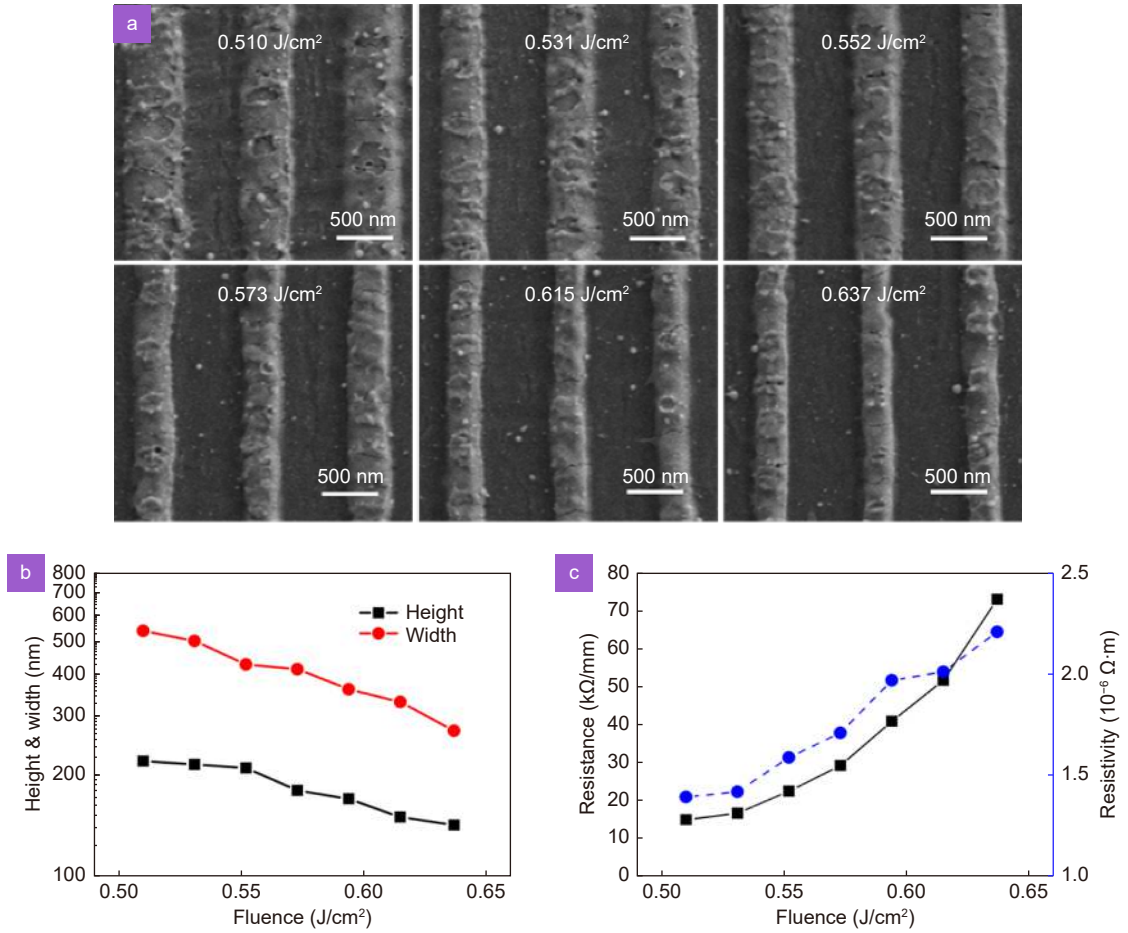

Fig. 8 | (**a**) SEM images of nanowires fabricated via laser direct writing with different fluences. (**b**) Height and width of nanowires with respect to the laser fluence. (**c**) Unit resistance and resistivity of nanowires with respect to the laser fluence.

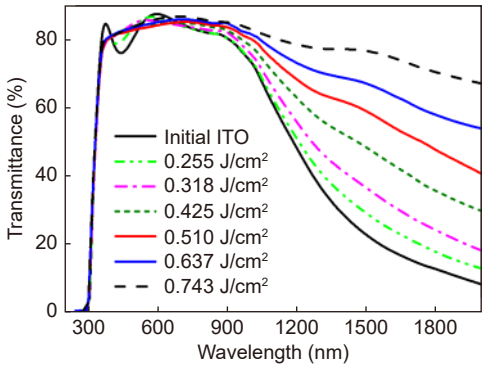

Fig. 9 | Transmission spectra of the ITO film after laser direct writing with different fluences at a constant scanning speed of 3 mm/s.

In the range of 0.510–0.637 J/cm², regular nanowires were formed on the ITO film, and the average transmittance in the infrared band increased to 54.48%–63.38% (156%–197% higher than that of the initial ITO film). Meanwhile, the transmittance in the visible band was slightly higher and more uniform. These results indicate that by adjusting the laser fluence, the transmittance of the ITO film in the infrared band can be increased significantly. Moreover, the electrical conductivity is well maintained. This is important for an ITO film with a regular LSFL as the transparent electrode of the photoelectric device in the infrared band.

Discussion

Regular LSFLs were fabricated on an ITO film irradiated by a laser with a fluence of 0.510 J/cm² at a scanning speed of 3 mm/s. An area of 10 μm × 10 μm was selected, and the element concentrations were analyzed using an SEM. As shown in Fig. 10(a–c), the spatial distributions of In and Sn were identical to those for the LSFL. In the point scanning mode, an EDS analysis was performed for the valley and ridge of the LSFL, respectively. Figure 10(d) presents the map sum spectra for the ridge of the LSFL. The concentrations of In and Sn were 4.01% and 1.76%, respectively, and the In/Sn concentration ratio was 2.28. For the initial ITO film with a thickness of 185 nm, the concentrations of In and Sn were 15.89% and

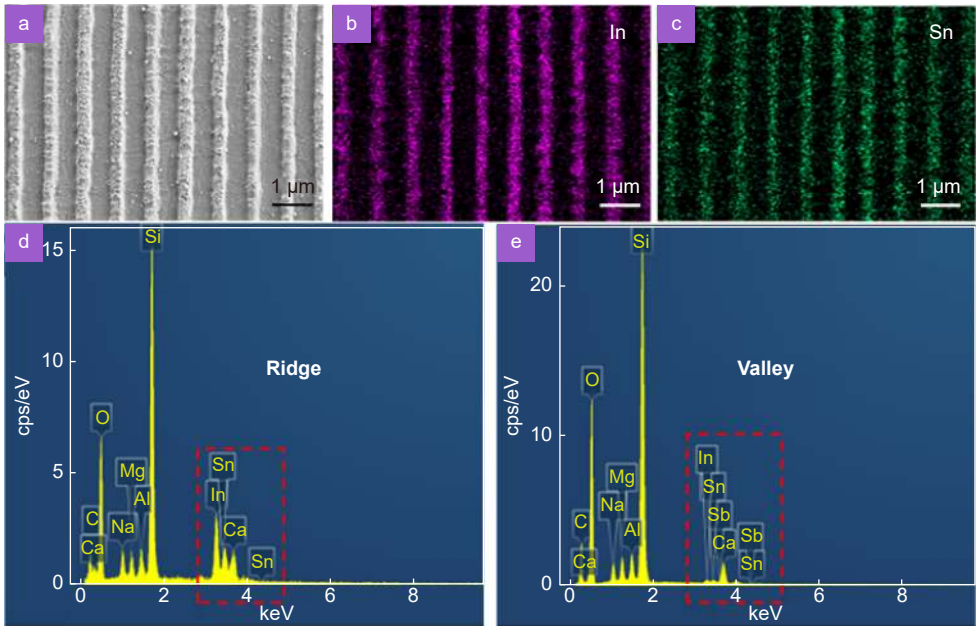

Fig. 10 | (**a–c**) Distributions of In and Sn for the ITO film with the LSFL; the scale bar represents 1 μm. Map sum spectra for the (**d**) ridge and (**e**) valley of the LSFL.

3.44%, respectively, and the In/Sn concentration ratio was 4.61. The ITO film was prepared by doping In_2O_3 with SnO_2, and the electrons released after Sn^{4+} replaced In^{3+} and the presence of $(O_2)^{2-}$ made the ITO film conductive[3]. Numerous studies have been performed on the effects of the In and Sn concentrations on the conductive properties of ITO films. The results indicate that the electrical conductivity of the ITO film changes little when the In concentration is changed from 3% to 15% and that the In and Sn concentration ratio varies in the range of 2–6[42–44]. These results explain why the regular LSFLs were good nanowires with a low resistivity of 1.395×10^{-6} Ω·m on average.

However, as shown in Fig. 10(e), the results differed for the valley of the LSFL. The In concentration was significantly reduced (to 0.66%), and the Sn concentration was only 1.14%. The In/Sn ratio was reduced to 0.58. The In concentration at the LSFL valley was very low, and the material exhibited a high resistance and even insulating properties. In previous studies, very small amounts of In and Sn penetrated the substrate material after the ITO film was completely ablated by the femtosecond laser; thus, In and Sn were still detected[19].

Figure 11(a) shows the concentrations of In and Sn and the In/Sn concentration ratio at the ridge and valley of the LSFL with respect to the laser fluence. When laser fluence was 0.212 J/cm², only periodic ablation appeared on the ITO film. The concentrations of In and Sn at the ridge of periodic ablation were reduced to 6.39% and 2.44%, respectively, and the In/Sn ratio was 2.85. With an increase in the laser fluence, the In and Sn concentrations decreased. In the range of 0.510–0.616 J/cm², the In and Sn concentrations remained at approximately 3.45% and 1.45%, respectively, and the In/Sn ratio was of 2.3. In these cases, the electrical conductivity of the LSFL nanowires was high. Surprisingly, when the laser fluence increased beyond 0.679 J/cm², the In and Sn concentrations and the In/Sn ratio were only slightly reduced, i.e., 3.35%, 1.45% and 2.3, respectively. As shown in Fig. 6, the resistance of the LSFL nanowires increased abruptly to infinity, mainly owing to the fracture of the LSFL. The results indicate that laser irradiation had little effect on the electrical conductivity of the ITO.

The In and Sn concentrations in the valley and the ratio of In/Sn with the increasing laser fluence are shown in Fig. 11(b). The three curves exhibited sharper declines than those for the ridge. When the laser fluence exceeded 0.510 J/cm², the In and Sn concentrations rapidly decreased to 0.66% and 1.14%, respectively. Thereafter, In and Sn were essentially absent from the valley of the LSFL, and the material exhibited as high resistance.

As shown in Fig. 8(c), the resistivity of the nanowires increased from 1.395×10^{-6} Ω·m to 2.210×10^{-6} Ω·m when the laser fluence increased from 0.510 J/cm² to 0.637 J/cm². However, the results in Fig. 11(a) indicate that the In and Sn concentrations were nearly constant,

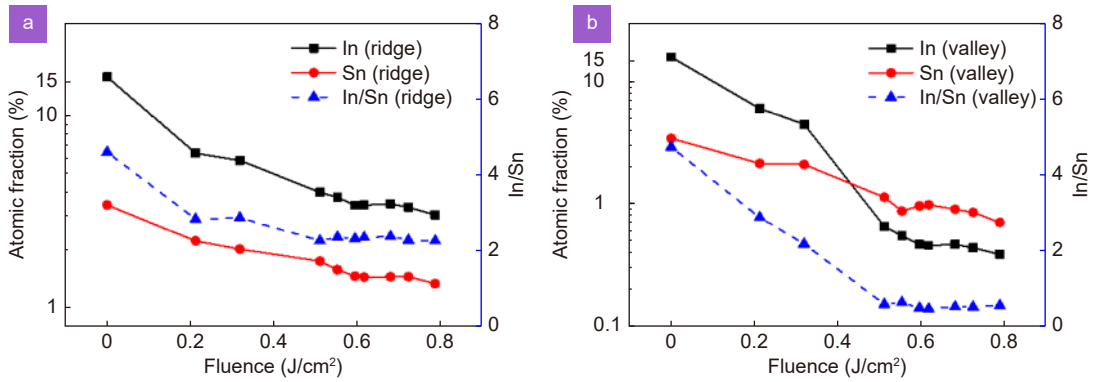

Fig. 11 | Concentrations of In and Sn and the In/Sn ratio at the (**a**) ridge and (**b**) valley of the LSFL with respect to the laser fluence.

suggesting that the resistivity of the nanowires should have been unchanged. To investigate this phenomenon, the In and Sn concentrations were measured with respect to the thickness of the ITO film, as shown in Fig. 12(a). As the thickness of the ITO film decreased from 260 nm to 50 nm, the In concentration decreased significantly (from 19.85% to 2.63%), and the Sn concentration decreased from 3.81% to 1.32%. This is mainly because the penetration depth in the EDS measurement was 600 nm, and more elements of the SiO_2 substrate material were detected with the decreasing of the thickness of the ITO film. Therefore, the reductions in the In and Sn concentrations at the ridge of the LSFL shown in Fig. 11(a) were partly caused by the larger amounts of ITO materials being ablated by the stronger laser.

Figure 12(b) presents the resistivity and sheet resistance with respect to the thickness of the ITO film. As the thickness of the ITO film decreased from 260 to 50 nm, the resistivity increased approximately linearly from 1.145×10^{-6} Ω·m to 1.774×10^{-6} Ω·m, which was an increase of 55%. The resistivity of the ITO film was not constant; it was higher for thinner films. The In and Sn concentrations of the 50-nm-thick ITO films were close to those at the ridge of the LSFL, and the resistivity of the ITO film was nearly equal to the average value for nanowires fabricated using lasers with fluences ranging from 0.510 J/cm² to 0.637 J/cm². These results explain the good electrical conductivity of the fabricated nanowires.

The results indicate that during the laser irradiation, the ITO-material removal caused by ablation reduced the height and width of the nanowires, which was the main reason for the increase in the resistivity. Therefore, the electrical conductivity of the ITO material is hardly affected during the laser fabrication of LSFLs.

Conclusions

Regular large-area LSFLs were fabricated on ITO films via femtosecond laser direct writing focused by a cylindrical lens. The effects of the laser fluence and scanning speed on the surface morphology of the ITO film were studied in detail. Periodic ablation, regular LSFLs, and partly damaged LSFLs were formed in sequence on the ITO films by increasing the laser fluence. Here, the scanning speed was 3 mm/s. Interestingly, regular large-area LSFLs were efficiently fabricated in the ITO film by changing the laser fluence in the range of 0.510–0.637 J/cm².

The anisotropic electrical conductivity of the

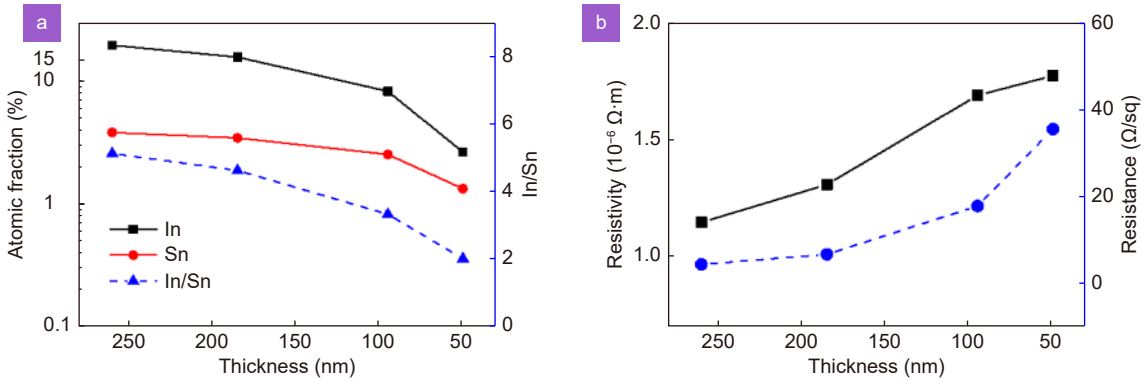

Fig. 12 | (**a**) Distributions of In and Sn and (**b**) resistivity and sheet resistance for ITO films with different thicknesses.

nanostructured ITO thin film was measured via the four-probe and dual-probe methods. The ratio of the anisotropic electrical conductivity of the periodic ablated ITO films was adjusted in the range of 1–10.8 by varying the laser fluence in the range of 0–0.488 J/cm^2. Surprisingly, the regular LSFL exhibited good properties as nanowires. The resistance of the nanowires could be tuned from 15 kΩ/mm to 73 kΩ/mm with a consistency of ±10% because the width and height both decreased as the laser fluence increased from 0.510 J/cm^2 to 0.637 J/cm^2. The element concentrations and the resistivities of the LSFL nanowires and the ITO film with different thicknesses were studied in detail. The results indicated that the resistivity of the LSFL nanowires was nearly equal to that of the initial ITO film. Thus, the resistivity of the LSFL nanowires was well maintained. Moreover, the average transmittance of the LSFL nanowires in the infrared band increased from 21.3% to 54.48%–63.38%. These LSFL nanowires have considerable potential for transparent electrodes of nano-optoelectronic devices–particularly in the NIR band.

References

1. Liu HY, Avrutin V, Izyumskaya N, Özgür Ü, Morkoç H. Transparent conducting oxides for electrode applications in light emitting and absorbing devices. *Superlattice Microst* **48**, 458–484 (2010).
2. Exarhos GJ, Zhou XD. Discovery-based design of transparent conducting oxide films. *Thin Solid Films* **515**, 7025–7052 (2007).
3. Ma ZZ, Li ZR, Liu K, Ye CR, Sorger VJ. Indium-tin-oxide for high-performance electro-optic modulation. *Nanophotonics* **4**, 198–213 (2015).
4. Kim H, Gilmore CM, Piqué A, Horwitz JS, Mattoussi H et al. Electrical, optical, and structural properties of indium–tin–oxide thin films for organic light-emitting devices. *J Appl Phys* **86**, 6451–6461 (1999).
5. Tahar RBH, Ban T, Ohya Y, Takahashi Y. Tin doped indium oxide thin films: electrical properties. *J Appl Phys* **83**, 2631–2645 (1998).
6. Parra-Barranco J, García-García FJ, Rico V, Borrás A, López-Santos C et al. Anisotropic in-plane conductivity and dichroic gold plasmon resonance in plasma-assisted ITO thin films e-beam-evaporated at oblique angles. *ACS Appl Mater Interfaces* **7**, 10993–11001 (2015).
7. Bonse J, Höhm S, Kirner SV, Rosenfeld A, Krüger J. Laser-induced periodic surface structures — a scientific evergreen. *IEEE J Sel Top Quant Electron* **23**, 9000615 (2017).
8. Shimotsuma Y, Kazansky PG, Qiu JR, Hirao K. Self-organized nanogratings in glass irradiated by ultrashort light pulses. *Phys Rev Lett* **91**, 247405 (2003).
9. Jia TQ, Chen H, Zhang YM. Photon absorption of conduction-band electrons and their effects on laser-induced damage to optical materials. *Phys Rev B* **61**, 16522–16529 (2000).
10. Zhang B, Tan DZ, Wang Z, Liu XF, Xu BB et al. Self-organized phase-transition lithography for all-inorganic photonic textures. *Light Sci Appl* **10**, 93 (2021).
11. Lin ZY, Liu HG, Ji LF, Lin WX, Hong MH. Realization of ~10 nm features on semiconductor surfaces via femtosecond laser direct patterning in far field and in ambient air. *Nano Lett* **20**, 4947–4952 (2020).
12. Zhang DS, Sugioka K. Hierarchical microstructures with high spatial frequency laser induced periodic surface structures possessing different orientations created by femtosecond laser ablation of silicon in liquids. *Opto-Electron Adv* **2**, 190002 (2019).
13. Zhang DS, Wu LC, Ueki M, Ito Y, Sugioka K. Femtosecond laser shockwave peening ablation in liquids for hierarchical micro/nanostructuring of brittle silicon and its biological application. *Int J Extrem Manuf* **2**, 045001 (2020).
14. Zhao B, Zheng X, Lei YH, Xie HB, Zou TT et al. High-efficiency-and-quality nanostructuring of molybdenum surfaces by orthogonally polarized blue femtosecond lasers. *Appl Surf Sci* **572**, 151371 (2022).
15. Chen L, Cao KQ, Li YL, Liu JK, Zhang SA et al. Large-area straight, regular periodic surface structures produced on fused silica by the interference of two femtosecond laser beams through cylindrical lens. *Opto-Electron Adv* **4**, 200036 (2021).
16. Zhang YC, Jiang QL, Cao KQ, Chen TQ, Cheng K et al. Extremely regular periodic surface structures in a large area efficiently induced on silicon by temporally shaped femtosecond laser. *Photonics Res* **9**, 839–847 (2021).
17. Zhou R, Huang TT, Lu YY, Hong MH. Tunable coloring via post-thermal annealing of laser-processed metal surface. *Appl Sci* **8**, 1716 (2018).
18. Liu HG, Lin WX, Hong MH. Surface coloring by laser irradiation of solid substrates. *APL Photonics* **4**, 051101 (2019).
19. Chen L, Cao KQ, Liu JK, Jia TQ, Li YL et al. Surface birefringence of regular periodic surface structures produced on glass coated with an indium tin oxide film using a low-fluence femtosecond laser through a cylindrical lens. *Opt Express* **28**, 30094–30106 (2020).
20. Zou TT, Zhao B, Xin W, Wang FY, Xie HB et al. Birefringent response of graphene oxide film structurized via femtosecond laser. *Nano Res* **15**, 4490–4499 (2022).
21. Cunha A, Serro AP, Oliveira V, Almeida A, Vilar R et al. Wetting behaviour of femtosecond laser textured Ti–6Al–4V surfaces. *Appl Surf Sci* **265**, 688–696 (2013).
22. Zhao YZ, Su YL, Hou XY, Hong MH. Directional sliding of water: biomimetic snake scale surfaces. *Opto-Electron Adv* **4**, 210008 (2021).
23. Su YL, Zhao YZ, Jiang SY, Hou XY, Hong MH. Anisotropic superhydrophobic properties of bioinspired surfaces by laser ablation of metal substrate inside water. *Adv Mater Interfaces* **8**, 2100555 (2021).
24. Reinhardt HM, Maier P, Kim HC, Rhinow D, Hampp N. Nanostructured transparent conductive electrodes for applications in harsh environments fabricated via nanosecond laser‐induced periodic surface structures (LIPSS) in indium–tin oxide films on glass. *Adv Mater Interfaces* **6**, 1900401 (2019).
25. Pan AF, Wang WJ, Liu B, Mei XS, Yang HZ et al. Formation of high-spatial-frequency periodic surface structures on indium-tin-oxide films using picosecond laser pulses. *Mater Des* **121**, 126–135 (2017).
26. Liu P, Wang WJ, Pan AF, Xiang Y, Wang DP. Periodic surface structures on the surface of indium tin oxide film obtained using

picosecond laser. *Opt Laser Technol* **106**, 259–264 (2018).
27. Solodar A, Cerkauskaite A, Drevinskas R, Kazansky PG, Abdulhalim I. Ultrafast laser induced nanostructured ITO for liquid crystal alignment and higher transparency electrodes. *Appl Phys Lett* **113**, 081603 (2018).
28. Cerkauskaite A, Drevinskas R, Solodar A, Abdulhalim I, Kazansky PG. Form-birefringence in ITO thin films engineered by ultrafast laser nanostructuring. *ACS Photonics* **4**, 2944–2951 (2017).
29. Miccoli I, Edler F, Pfnür H, Tegenkamp C. The 100th anniversary of the four-point probe technique: the role of probe geometries in isotropic and anisotropic systems. *J Phys Condens Matter* **27**, 223201 (2015).
30. Hong S, Lee H, Yeo J, Ko SH. Digital selective laser methods for nanomaterials: from synthesis to processing. *Nano Today* **11**, 547–564 (2016).
31. Zhang FZ, Chen L, Zhang YC, Jiang QL, Feng DH et al. High-performance birefringence of periodic nanostructures in FTO thin film fabricated by IR-UV femtosecond laser. *Front Phys* **10**, 861389 (2022).
32. Cao KQ, Chen L, Wu HC, Liu JK, Cheng K et al. Large-area commercial-grating-quality subwavelength periodic ripples on silicon efficiently fabricated by gentle ablation with femtosecond laser interference via two cylindrical lenses. *Opt Laser Technol* **131**, 106441 (2020).
33. Cheng K, Liu JK, Cao KQ, Chen L, Zhang YC et al. Ultrafast dynamics of single-pulse femtosecond laser-induced periodic ripples on the surface of a gold film. *Phys Rev B* **98**, 184106 (2018).
34. Zhou K, Jia X, Jia TQ, Cheng K, Cao KQ et al. The influences of surface plasmons and thermal effects on femtosecond laser-induced subwavelength periodic ripples on Au film by pump-probe imaging. *J Appl Phys* **121**, 104301 (2017).
35. Bian QM, Yu XM, Zhao BZ, Chang ZH, Lei ST. Femtosecond laser ablation of indium tin-oxide narrow grooves for thin film solar cells. *Opt Laser Technol* **45**, 395–401 (2013).
36. Fernandes SA, Schoeps B, Kowalick K, Nett R, Esen C et al. Femtosecond laser ablation of ITO/ZnO for thin film solar cells. *Phys Procedia* **41**, 802–809 (2013).
37. Cheng CW, Lee IM, Chen JS. Femtosecond laser processing of indium-tin-oxide thin films. *Opt Lasers Eng* **69**, 1–6 (2015).
38. Hertwig A, Martin S, Krüger J, Kautek W. Interaction area dependence of the ablation threshold of ion-doped glass. *Thin Solid Films* **453–454**, 527–530 (2004).
39. Jia TQ, Baba M, Suzuki M, Ganeev RA, Kuroda H et al. Fabrication of two-dimensional periodic nanostructures by two-beam interference of femtosecond pulses. *Opt Express* **16**, 1874–1878 (2008).
40. Kim H, Piqué A, Horwitz JS, Mattoussi H, Murata H et al. Indium tin oxide thin films for organic light-emitting devices. *App Phys Lett* **74**, 3444–3446 (1999).
41. Zhao J, Ding XH, Miao JH, Hu JF, Wan H et al. Improvement in light output of ultraviolet light-emitting diodes with patterned double-layer ITO by laser direct writing. *Nanomaterials* **9**, 203 (2019).
42. Shigesato Y, Hayashi Y, Haranoh T. Doping mechanisms of tin - doped indium oxide films. *Appl Phys Lett* **61**, 73–75 (1992).
43. Jia JJ, Takaya A, Yonezawa T, Yamasaki K, Nakazawa H et al. Carrier densities of Sn-doped In_2O_3 nanoparticles and their effect on X-ray photoelectron emission. *J Appl Phys* **125**, 245303 (2019).
44. Petukhov IA, Shatokhin AN, Putilin FN, Rumyantseva MN, Kozlovskii VF et al. Pulsed laser deposition of conductive indium tin oxide thin films. *Inorg Mater* **48**, 1020–1025 (2012).

Acknowledgements

We are grateful for financial supports from the Ministry of Science and Technology of China (Grant No. 2021YFA1401100), and National Natural Science Foundation of China (Grant Nos. 12074123, 11804227, 91950112), and the Foundation of 'Manufacturing beyond limits' of Shanghai.

Author contributions

Q. L. Jiang performed the experiment and measurements under the guidance of T. Q. Jia and L. Chen. J. K. Liu, Y. C. Zhang, S. A. Zhang, D. H. Feng, Z. R. Sun, P Zhou, Q Wang and H. X. Xu gave important suggestions to this work

Competing interests

The authors declare no competing financial interests.

Supplementary information

The measurement methods of electrical properties of ITO film and resistance of LSFL nanowires are presented in Appendix I.
https://doi.org/10.29026/oes.2023.220002